

Received 13 April 2025; revised 13 May 2025; accepted 3 June 2025. Date of publication 11 June 2025; date of current version 27 June 2025.

Digital Object Identifier 10.1109/OJCOMS.2025.3578864

Energy Consumption Modeling for Wi-Fi HaLow Networks

ZHIQIANG XU^{ID}, LUKE KANE^{ID} (Member, IEEE), VICKY LIU^{ID}, MATTHEW MCKAGUE^{ID}, AND YUEFENG LI^{ID}

Faculty of Science, Queensland University of Technology, Brisbane, QLD 4000, Australia

CORRESPONDING AUTHOR: Z. XU (e-mail: zhiqiang.xu@hdr.qut.edu.au)

This work was supported by the Queensland University of Technology.

ABSTRACT Wi-Fi HaLow (IEEE 802.11ah) has emerged as a promising solution which can support Internet of Things (IoT) applications where energy efficiency and extended coverage are important. A key feature of Wi-Fi HaLow is the Target Wake Time (TWT) mechanism, which allows devices to schedule wake-up times, significantly reducing IDLE listening and energy consumption. However, there is currently no energy consumption model, leaving a gap in calculating how much energy a device actually consumes in a real network. This study aims to bridge this gap by developing a forecast model to accurately predict the energy consumption of devices with TWT enabled. The proposed model is then validated through experimental measurements using real Wi-Fi HaLow-compatible devices, ensuring an accurate representation of practical energy consumption. This research provides empirical insights and recommendations for optimizing network configurations in battery-constrained environments. In particular, the proposed energy consumption model can assist businesses in accurately estimating and managing energy usage, which is essential for cost-effective planning and improving operational efficiency in real-world IoT deployments.

INDEX TERMS Wi-Fi HaLow, IEEE 802.11ah, target wake time (TWT), energy consumption, Internet of Things (IoT), wireless networks.

I. INTRODUCTION

THE Internet of Things (IoT) has enabled a wide range of innovative applications across domains such as smart agriculture, industrial automation, and environmental monitoring [1]. While IoT systems can bring significant benefits, they also present significant challenges, with efficient energy consumption being one of the main concerns [2], [3]. As IoT devices are often battery-powered and expected to operate over long periods without human intervention, minimizing energy usage is crucial for extending device lifespan and ensuring reliable operation. This is particularly important in remote or hard-to-reach environments, where frequent battery replacement is impractical. Consequently, optimizing energy efficiency not only enhances sustainability but also reduces long-term maintenance costs and operational expenses in large-scale IoT deployments [4], [5].

Several low-power communication protocols have been developed to meet the energy demands of IoT systems. Among them, technologies such as LoRa, Zigbee, Bluetooth Low Energy (BLE), and Sigfox each present specific

advantages and disadvantages [6], [7], [8]. For instance, LoRa can operate over long distances using minimal energy due to its use of low data rate modulation and long symbol duration, which enable reliable signal decoding over extended distances. However, its throughput may make it unsuitable for certain real-time applications [7]. BLE is energy-efficient for short-range communication but struggles with scalability in dense networks. Zigbee offers improved scalability but with limited range and bandwidth [8]. While each protocol is tailored to a specific constraint, none can simultaneously meet the combined demands of coverage, data throughput, and energy longevity.

Wi-Fi HaLow, also known as IEEE 802.11ah, aims to overcome some of the limitations of existing low-power communication protocols. By operating in the sub-GHz frequency band, Wi-Fi HaLow achieves a greater communication range and better penetration through obstacles when compared with traditional Wi-Fi, making it suitable for both urban and rural environments [9]. Wi-Fi HaLow is specifically designed to address the energy efficiency

challenges in IoT networks through several mechanisms. These include optimized modulation techniques and reduced overhead protocols, which lower the power consumption during transmissions [1], [10]. Moreover, power-saving functions allow for adaptive communication, enabling devices to switch between active and low-power states efficiently based on data transmission needs. The combination of lower operating frequencies and energy-efficient MAC protocols ensures that even high-throughput applications, such as video streaming, can be accommodated without compromising battery life [11], [12]. In contrast to conventional protocols, these features position Wi-Fi HaLow as a promising candidate for IoT deployments, especially in remote environments, where both energy efficiency and reliable communication are critical [11], [13], [14], [15]. Nonetheless, Wi-Fi HaLow also has practical limitations, including a lack of a mature ecosystem, limited chipset availability and limited group scheduling flexibility.

A key energy-saving feature that distinguishes Wi-Fi HaLow is the introduction of the Target Wake Time (TWT) mechanism. TWT allows station (STA) to negotiate wake-up schedules with an access point (AP), thereby minimizing IDLE listening—a primary cause of energy drain [14], [16], [17]. TWT is especially suitable for scenarios requiring long operational lifespans with minimal human intervention, such as agricultural monitoring systems, remote industrial sensors, and environmental data collection networks [18]. These deployments often operate in locations with limited physical access or constrained maintenance resources, making energy efficiency critical. Several studies have verified the energy-saving potential of TWT [19], [20], which indicates that TWT can reduce IDLE listening and extend battery life in IoT scenarios with low to moderate data traffic.

Despite the theoretical advantages of TWT, there remains a lack of practical understanding of its energy impact in real-world deployments. Most existing studies on TWT rely on simulation. Simulation-based research on TWT provides several advantages, such as enabling the exploration of numerous network configurations under controlled conditions and offering a cost-effective way to test various scenarios without the need for physical deployments [18], [19], [20]. However, simulations inherently rely on simplified assumptions that often treat current consumption as constant, ignoring how it varies with bandwidth and Modulation and Coding Scheme (MCS) [7], [21], [22], [23], [24], [25]. This overlooks the dynamic power behavior of real Wi-Fi HaLow devices, where current fluctuates significantly with different configurations. These limitations highlight the importance of conducting energy studies based on real hardware and deployment environments. To the best of our knowledge, no prior study has experimentally investigated the energy behavior of TWT using physical devices, and no validated energy consumption model exists to quantify how much energy is actually consumed in real-world Wi-Fi HaLow deployments. This gap limits the ability of researchers and practitioners to accurately estimate

the energy cost of enabling TWT, and to make informed decisions when designing or deploying low-power Wi-Fi HaLow systems.

To address this gap, the objective of this study is to develop an accurate and empirically validated energy consumption model for Wi-Fi HaLow stations operating under the TWT mechanism. The model is based on real measurements collected from commercial Wi-Fi HaLow hardware communicating in realistic environments. By capturing the nuances of hardware behavior that simulations may overlook, such as power leakage [26] or startup current drawn [27], [28], the proposed model provides a more realistic understanding of energy performance.

Developing such a model is of both scientific and practical significance. On one hand, it provides a foundation for future research on energy-aware MAC protocol design and system-level power optimization. On the other hand, it offers concrete benefits for practitioners and system integrators. Accurate energy modeling assists businesses in forecasting energy requirements, optimizing deployment strategies, and implementing effective energy management policies, thereby supporting long-term cost control and improving operational efficiency in IoT-based services and infrastructures.

The main contributions of this study are as follows:

- An accurate forecast model is developed to predict the energy consumption of Wi-Fi HaLow devices with TWT enabled, considering traffic load parameters such as data size and network parameters such as MCS and bandwidth.
- The proposed energy consumption model is validated and proven to be accurate through experiments using actual Wi-Fi HaLow devices rather than relying on simulations.
- Practical recommendations based on empirical results are provided to optimize energy consumption for Wi-Fi HaLow devices, offering insights for manufacturers, researchers, and network administrators to enhance energy-efficient IoT network deployments.

The remainder of this paper is organized as follows: Section II describes the experimental setup, including hardware components and measurement methodology. Section III details the development of the energy consumption model under TWT operation. Section IV analyzes experimental results, model validation, influencing factors, and practical insights. Section V discusses model advantages, limitations, and future extensions for real-world applicability. Finally, Section VI concludes the paper and outlines potential directions for future work. A list of abbreviations used throughout this paper is provided in Table 1 for reference.

II. EXPERIMENTAL SETUP

This section describes the experimental setup used to evaluate the energy consumption of an STA under the TWT mechanism in Wi-Fi HaLow networks. It includes a detailed explanation of the hardware components used, an overview of the TWT implementation in the MM6108 chip, and the methodology adopted for precise energy consumption

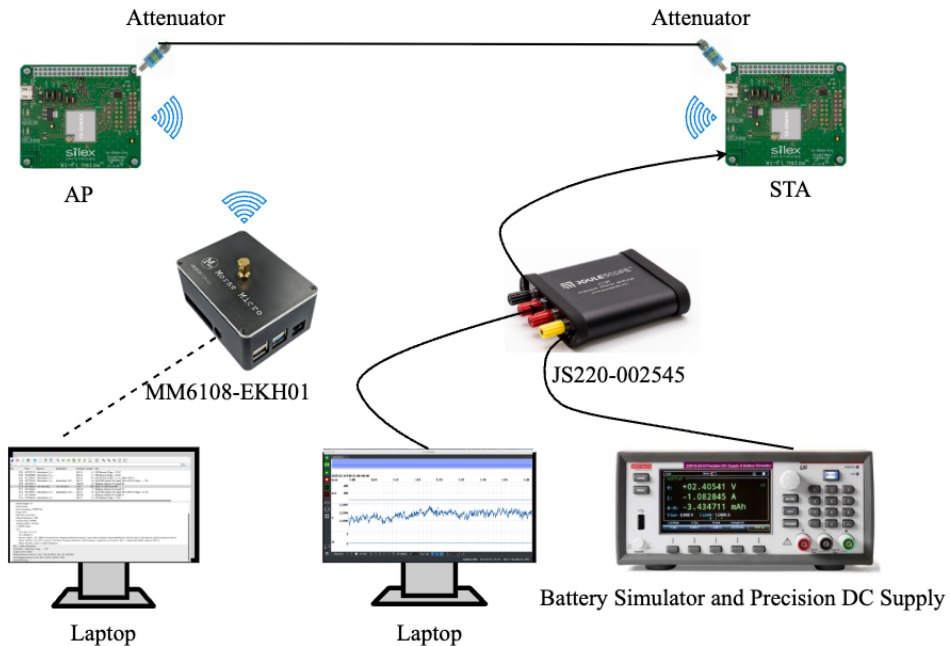


FIGURE 1. Experimental setup for energy consumption analysis in Wi-Fi HaLow networks.

TABLE 1. List of abbreviations used in this paper.

Abbreviation	Full Form
IoT	Internet of Things
TWT	Target Wake Time
BLE	Bluetooth Low Energy
MCS	Modulation and Coding Scheme
AP	Access Point
STA	Station
MAC	Medium Access Control
FEM	Front-End Module
MCU	Microcontroller Unit
PSDU	PLCP Service Data Unit
PLCP	Physical Layer Convergence Protocol
RF	Radio Frequency
GI	Guard Interval
ACK	Acknowledgement
SoC	System-on-Chip
TX	Transmission
RX	Reception
QoS	Quality of Service
TIM	Traffic Indication Map
DTIM	Delivery Traffic Indication Message
AE	Absolute Error
RE	Relative Error

measurements. These elements together support the analysis presented in the subsequent sections.¹

A. HARDWARE COMPONENTS

To conduct precise energy measurements, a specialized hardware setup is deployed, as shown in Figure 1. The system consists of the following key components:

- 802.11ah-Enabled Devices (AP and STA): The experiment utilizes two Silex SX-SDMAH Wi-Fi HaLow modules, one acting as an AP and the other as an STA. The SX-SDMAH module, based on the Morse Micro MM6108 chipset, is a Wi-Fi HaLow module designed for long-range, low-power wireless communication. It supports a maximum channel bandwidth of 8 MHz and a maximum transmission power of +24 dBm. The module operates at three voltage levels: VDD (3.3V), VDDIO (3.3V), and VDDFEM (3.3V or 5V for the U.S. version). VDD supplies power to the core chip, enabling protocol execution and data processing. VDDIO powers the SDIO/SPI interface, facilitating communication between the module and the host system. VDDFEM provides power to the RF front-end module (FEM), which is responsible for wireless transmission.
- MM6108-EKH01: The MM6108-EKH01, based on the Morse Micro MM6108 chipset, is employed as a packet capture and analysis tool. This device is configured in sniffing mode to capture and decode the Wi-Fi HaLow communication between the AP and STA. The captured data includes management frames, data frames, control frames, and TWT negotiation packets, providing insights into protocol behavior and transmission timing. These packets can be displayed and analyzed in real time using Wireshark software on a connected laptop. By analyzing these packets, we can correlate power consumption patterns with different operational states of the STA.
- MM6108: The Morse Micro MM6108 is a fully integrated Wi-Fi HaLow system-on-chip (SoC) that supports Radio, PHY, and MAC layer functionalities.

TABLE 2. Wi-Fi HaLow modulation and coding scheme for MM6108.

MCS Index	Modulation Scheme	Coding Rate	1 MHz (kbps)	2 MHz (kbps)	4 MHz (kbps)	8 MHz (kbps)
10	BPSK	1/2 x 2	167	N/A	N/A	N/A
0	BPSK	1/2	333	722	1500	3250
1	QPSK	1/2	667	1444	3000	6500
2	QPSK	3/4	1000	2167	4500	9750
3	16-QAM	1/2	1333	2889	6000	13000
4	16-QAM	3/4	2000	4333	9000	19500
5	64-QAM	2/3	2667	5778	12000	26000
6	64-QAM	3/4	3000	6500	13500	29250
7	64-QAM	5/6	3333	7222	15000	32500

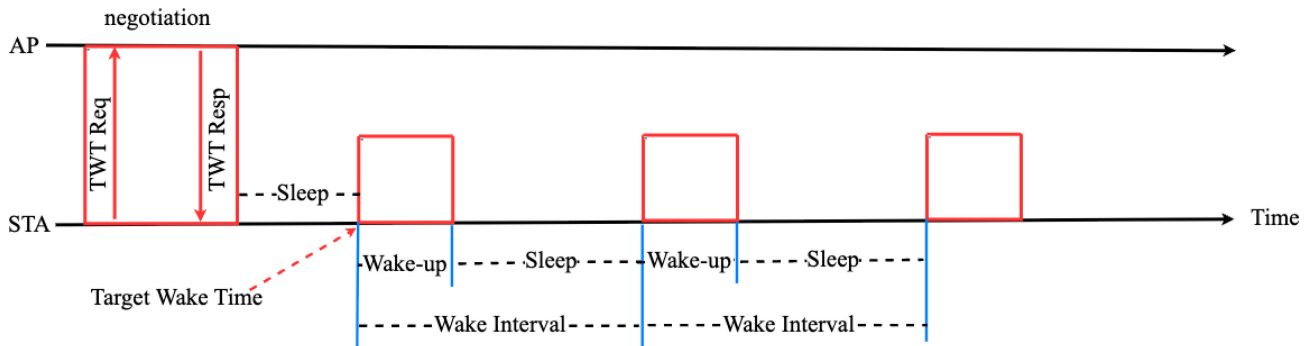


FIGURE 2. TWT Operation in MM6108: Implicit mode with individual agreement. The STA establishes a single-user TWT session through a negotiation with the AP and subsequently follows a periodic wake-up schedule based on a fixed interval.

In this experiment, the MM6108 firmware version used is rel_1_10_2_2023_Nov_22. While the MM6108 follows the IEEE 802.11ah standard, it exhibits some implementation-specific differences, with MCS support being one of them. The Wi-Fi HaLow standard defines MCS indices ranging from 0 to 9, supporting modulation schemes up to 256-QAM (MCS 8 and 9), whereas MM6108 only supports MCS indices from 0 to 7, as detailed in Table 2. An exception is MCS 10, which is supported in both the standard and MM6108, but only when the channel bandwidth is 1 MHz.

- Joulescope: The Joulescope JS220-002545 is used to precisely measure and analyze the current, voltage, and energy consumption of the STA during different operational states, including IDLE, transmission (TX), and reception (RX). It supports ± 15 V, up to ± 3 A current range with 0.5 nA resolution. More importantly, it provides high-resolution measurements of state transitions, such as the sleep-to-wake-up process. This enables a comprehensive evaluation of the STA's power behavior under the TWT mechanism, facilitating accurate calculations of energy consumption across entire TWT wake interval.
- Battery Simulator and Precision DC Supply: A Keithley 2281S-20-6 device was used to provide a stable and controlled power source to the STA. It supports up to 20V / 6A output and includes built-in battery simulation capabilities, enabling consistent and accurate energy measurements during experiments.

- Attenuators: To mitigate potential interference and maintain a stable wireless environment, CATTEN-0200 20 dB RF attenuators (Crystek Microwave) were used at both AP and STA to ensure stable signal strength. Each attenuator supports operation from DC to 3 GHz, with $50\ \Omega$ impedance, 0.5 W rated power, and ± 1 dB attenuation tolerance. These attenuators help control the signal strength and ensure accurate measurements by reducing unwanted fluctuations in received signal power.

B. OVERVIEW OF TWT IN MM6108

The TWT implementation in MM6108 differs from the Wi-Fi HaLow standard in several key aspects. The MM6108 supports only implicit TWT scheduling, where the STA calculates its next wake-up time using a fixed interval, resulting in a periodic and predictable wake-up schedule. Additionally, only announced TWT flows are supported, requiring the AP to wait for a Quality of Service (QoS) Null frame from the STA before transmitting buffered data. Furthermore, MM6108 only allows individual TWT agreements, meaning each STA establishes a one-to-one TWT session with the AP, without support for broadcast or group-based TWT.

As shown in Figure 2, which illustrates the macro-level TWT operation, the TWT operation begins with a negotiation phase, where the STA requests a wake-up schedule from the AP through a TWT Request frame, and the AP responds with a TWT Response frame, establishing an agreed wake

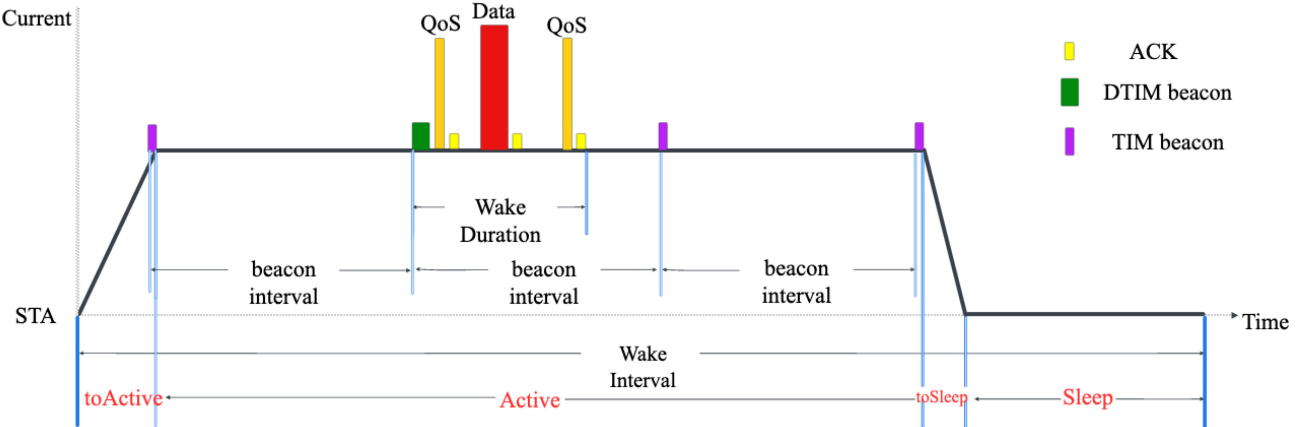


FIGURE 3. Current consumption of the STA core chip during a TWT wake interval. The core chip remains active throughout the wake interval to handle beacon reception and frame exchanges.

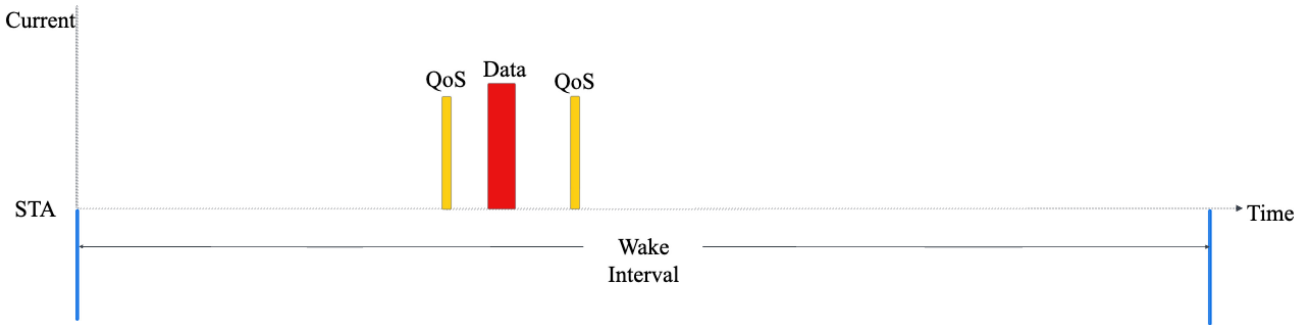


FIGURE 4. Current consumption of the STA FEM during a TWT wake interval. The FEM activates only during frame transmission, producing brief current spikes aligned with uplink QoS and data frames, and remains off otherwise.

interval. After this negotiation, the STA enters a periodic sleep-wake cycle, waking up only at the designated target wake times to exchange data. By following this predictable schedule, TWT minimizes unnecessary IDLE listening, significantly reducing power consumption compared to traditional contention-based wake-up mechanisms.

To gain a more detailed understanding of the operation of the TWT mechanism, we employed two complementary approaches: real-time current measurement and packet-level analysis. Joulescope was used to capture fine-grained current consumption patterns, while packet analysis was conducted using the MM6108-EKH01 module in sniffer mode. The packet captures allowed us to identify the specific types, sequence, and number of frames exchanged during each wake interval. By analyzing these packets, we directly correlate protocol events with real-time current fluctuations, enabling detailed energy profiling of the STA during TWT operation. This joint approach reveals how packet exchanges and device behavior influence energy consumption in practical deployments.

Figure 3 illustrates the current consumption profile of the core chip throughout a complete TWT cycle, it reveals four distinct phases that characterize TWT operation. In the toActive phase, the STA transitions from sleep to an active state. The Active phase involves data transmission and

reception, where the STA transmits Quality of Service (QoS) frames and data frames while receiving Traffic Indication Map (TIM) beacons, Delivery Traffic Indication Message (DTIM) beacons, and Acknowledgment (ACK) frames, as specified by the TWT agreement. After that, the toSleep phase begins, during which the STA stops communication and prepares to return to sleep mode. Finally, during the Sleep phase, the STA remains in a low-power state until the next scheduled wake interval. By monitoring the current consumption across these phases, we can precisely track how the TWT mechanism structures STA activity.

While the core chip's current consumption reflects the entire TWT operation, the FEM provides a more focused perspective, capturing only the process related to wireless transmission, as shown in Figure 4. Therefore, when analyzing the data transmission process and its energy consumption under TWT, it is essential to consider both the core chip and FEM.

C. METHODOLOGY OF ENERGY CONSUMPTION MEASUREMENT

To ensure accurate and reliable energy consumption analysis, this study operates under the assumption that all data exchanges occur successfully without retransmissions or

transmission failures. This assumption is necessary to isolate the impact of TWT scheduling and transmission parameters from external factors such as packet loss, interference, or retransmissions, which could lead to inconsistent energy measurement results. To reasonably support this assumption, a tightly controlled experimental environment was established. The SX-SDMAH modules were configured to operate at their maximum transmission power of 24 dBm to ensure a stable and robust communication link between the AP and STA. Additionally, experiments were conducted in an interference-free indoor setting with a fixed ambient temperature of 25°C, and attenuators were used to prevent signal overloading and to stabilize the received signal strength. These measures effectively minimized environmental uncertainties and allowed reproducible and phase-specific power profiling under ideal conditions.

Regarding the time frame for energy consumption measurement, the focus is placed on energy usage during a single wake interval after the TWT agreement has been established. As illustrated in Figure 2, once the TWT negotiation phase is completed, the STA follows a periodic wake-up and sleep schedule based on the agreed wake intervals. Since this behavior repeats in a predictable manner throughout the TWT session, measuring energy consumption over one complete wake interval provides an accurate representation of the overall energy usage across multiple cycles.

Regarding the modules selected for energy consumption measurement, the MM6108 core chip and the RF FEM are analyzed as they represent the primary power-consuming components influenced by TWT scheduling. In contrast, the VDDIO interface domain and Microcontroller Unit (MCU)-related power (e.g., packet processing, encryption) are excluded to avoid conflating unrelated system activity. Joulescope measurements under VDDIO show that transmission energy varies only slightly with packet size (e.g., 7 μ J for 500 bytes and 12 μ J for 1000 bytes) and wake-up phase energy shows only minor variations across different MCS levels and bandwidth settings. Furthermore, VDDIO power patterns are often influenced by asynchronous host-side activity (e.g., SPI exchanges), which are unrelated to the TWT mechanism. Including such effects would complicate the energy measurement without offering clearer insight into the energy behavior of TWT scheduling. Therefore, to accurately characterize the energy impact of the TWT mechanism itself, the scope of this study is limited to the core chip and FEM, which are directly responsible for the energy usage of the STA under TWT operation.

III. ENERGY CONSUMPTION MODELING UNDER TWT OPERATION

This section presents a detailed energy consumption model for the STA during a single wake interval, denoted as t_{interval} . Based on the phase classification introduced in Section II, the operation of the core chip is divided into four distinct phases: toActive, Active, toSleep, and Sleep, as shown in

Figure 3. These phases represent the complete activity cycle of the STA within one wake interval and serve as the basis for modeling the core chip's energy consumption.

The energy consumed by the core chip across the four operational phases is denoted as E_{Core} , which is calculated as the sum of the energy consumed in each phase. In parallel, the energy consumption of the FEM is modeled independently. Unlike the core chip, the FEM is only active during the data transmission, as shown in Figure 4. Its energy usage, denoted as E_{FEM} , is calculated separately based on the transmission activities. Therefore, the total energy consumption E of the STA during one complete wake interval is the sum of the core chip and FEM energy consumption.

The subsequent subsections present the modeling of each operational phase for the core chip, followed by a separate modeling of the FEM's energy consumption during data transmission.

A. ENERGY CONSUMPTION OF TO ACTIVE PHASE

The toActive phase primarily involves the STA powering on essential hardware components, maintaining readiness to synchronize with the AP, and receiving TIM beacon. Based on the information contained in these beacon—such as MCS and bandwidth—the STA adjusts its operating parameters accordingly.

The duration and energy consumption of the toActive phase are influenced by various factors, including network parameters (e.g., MCS and bandwidth), TWT-related parameters (e.g., TWT interval and beacon interval), and the hardware characteristics of the STA. These dependencies make it challenging to derive a precise energy consumption model using theoretical formulas alone.

To address this complexity, extensive measurements were conducted on the device to quantify the toActive phase's energy consumption and time. The results show minimal fluctuations, with the values varying within a narrow range. Based on 50 measurement iterations, the average duration of the toActive phase was determined to be 8.5 ms, with an energy consumption of 0.55 mJ. These measurements provide reliable and representative values for analyzing the energy profile of this phase. We define the time interval of the toActive phase as t_{toActive} and the energy consumption as E_{toActive} . These are expressed as:

$$t_{\text{toActive}} = 8.5 \text{ ms}, \quad (1)$$

$$E_{\text{toActive}} = 0.55 \text{ mJ}. \quad (2)$$

B. ENERGY CONSUMPTION OF ACTIVE PHASE

As shown in Figure 3, after the STA enters Active phase, it initially remains in an IDLE state until the arrival of the DTIM beacon. Upon receiving the beacon, the STA sends a QoS Null frame to the AP, signaling that it has woken up and is ready to initiate data exchange. The STA then transmits data to the AP, and before the wake duration ends, it sends another QoS Null frame to the AP, notifying its intent to

transition to sleep. These two QoS Null frames are identical in size but differ in their flags field. It is worth noting that whenever the STA sends any type of frame, whether a Data frame or a QoS Null frame, it always receives an ACK from the AP to confirm successful transmission.

In the SX-SDMAH module used in this study, the wake duration is defined as the period from the reception of the DTIM beacon to the completion of the ACK frame received in response to the second QoS Null frame transmission. After the wake duration ends, the STA waits for two consecutive TIM beacons, and upon receiving the second TIM beacon, it officially begins its transition to the sleep state.

To calculate the energy consumption of the Active phase, it is essential to determine the energy consumed by the STA in its IDLE, transmitting, and receiving states separately. The voltage, denoted as V , is preconfigured and remains constant, while the current for each state can be measured using the Joulescope. We denote the currents for the IDLE, transmitting, and receiving states as I_{IDLE} , I_{TX} , and I_{RX} , respectively. Therefore, the primary task is to accurately determine the duration of each state.

The duration of each state is determined by analyzing the frame structure exchanged during the Active phase. The size of each frame involved in the transmitting and receiving states is obtained by analyzing the captured packets. To determine the time duration of each frame, if the captured packet includes all necessary PHY and MAC parameters (e.g., preamble, bandwidth, MCS, guard interval), we calculate the transmission or reception duration using the formulas in IEEE 802.11ah standard [29]. This approach enhances model precision and reproducibility. In cases where such parameters are unavailable from the packet information, we perform multiple real-time measurements using Joulescope and use the averaged value to represent the frame duration, ensuring practical accuracy.

We now proceed to analyze the energy consumption for the transmitting, receiving, and IDLE states individually in the following three sub-sections.

1) TRANSMITTING STATE

To calculate the energy consumption during the transmitting state, it is essential to first determine the transmission duration. For the MM6108, two different transmission modes are utilized: S1G_1M preamble with long GI and S1G_SHORT preamble with short Guard Interval (GI). Each mode requires a specific formula to calculate the transmission time, considering various parameters related to the physical layer and encoding.

For the S1G_1M preamble with long GI, the transmission duration (T_{IM}) is given by:

$$T_{\text{IM}} = T_{\text{PREAMBLE}} + T_{\text{SIG}} + T_{\text{SYML}} \cdot N_{\text{SYM}}. \quad (3)$$

For the S1G_SHORT preamble with short GI, the transmission duration (T_{SHORT}) is calculated as:

$$T_{\text{SHORT}} = T_{\text{PREAMBLE}} + T_{\text{SIG}} + T_{\text{SYML}} + T_{\text{SYMS}} \cdot (N_{\text{SYM}} - 1). \quad (4)$$

Formulas (3) and (4) are adopted from the IEEE 802.11ah standard [29]. The time-related parameters involved, such as T_{PREAMBLE} , T_{SIG} , T_{LTF} , T_{SYML} , and T_{SYMS} , and the calculation of N_{SYM} are defined in Section 23.4.3 of the IEEE 802.11ah standard. It is important to note that when computing the transmission time, the GI value should be replaced with the actual settings. All the time-related parameters within the equations are directly influenced by the selected GI.

During the Active phase, the STA transmits two QoS Null frames and one Data frame, where the Data frame specifically refers to “Data” as defined within the broader category of Data Frames. Although the QoS Null frame is labeled as “no data” in its packet information, it is not a Null Data Packet. Measurements on the actual device reveal that the Physical Layer Convergence Protocol (PLCP) Service Data Unit (PSDU) length of the QoS Null frame is 30 bytes.

When transmitting, the QoS Null frames are transmitted using the S1G_1M preamble with long GI mode. For the data frame, the transmission mode depends on the bandwidth: at 1 MHz, the S1G_1M preamble with long GI mode is used, while at 2 MHz, 4 MHz, and 8 MHz, the S1G_SHORT preamble with short GI mode is adopted. Let the transmission time for a QoS Null frame and a Data frame be denoted as t_{QoS} and t_{Data} , respectively. The total transmission time t_{TX} can then be expressed as:

$$t_{\text{TX}} = 2 \cdot t_{\text{QoS}} + t_{\text{Data}}. \quad (5)$$

Based on the transmission time t_{TX} , the energy consumption during the transmitting state, denoted as E_{TX} , can be expressed as:

$$E_{\text{TX}} = I_{\text{TX}} \cdot t_{\text{TX}} \cdot V. \quad (6)$$

where V is the supply voltage, I_{TX} is the transmission current, and t_{TX} is the total transmission duration.

2) RECEIVING STATE

The duration of the Receiving state is determined by the time spent receiving one DTIM beacon, two TIM beacons, and three ACK frames. For ACK frames, it is not feasible to calculate the reception time using the formula specified in IEEE 802.11ah standard [29], as the captured packet information does not provide the necessary parameter values required for computing the reception time. To overcome this limitation, we conducted measurements on the SX-SDMAH module using the Joulescope. Specifically, for various MCS and bandwidth configurations, the time required to receive three ACK frames was measured 50 times, and the average value was used. Based on these measurements, the time to receive three ACK frames was determined to be 1 ms, with an energy consumption of 0.1 mJ. We denote the duration of receiving three ACK frames as t_{ACK} , and the corresponding energy consumption as E_{ACK} . These values are given by:

$$t_{\text{ACK}} = 1 \text{ ms}, \quad (7)$$

$$E_{\text{ACK}} = 0.1 \text{ mJ}. \quad (8)$$

TABLE 3. Time and energy consumption for TIM and DTIM beacons across different bandwidths.

Parameter	bandwidth (MHz)	Value
TIM Time	1	1.07ms
	2	1.15ms
	4	1.15ms
	8	1.10ms
TIM Energy	1	0.12mJ
	2	0.13mJ
	4	0.16mJ
	8	0.16mJ
DTIM Time	1	2.87ms
	2	2.94ms
	4	2.95ms
	8	2.90ms
DTIM Energy	1	0.31mJ
	2	0.34mJ
	4	0.40mJ
	8	0.42mJ

For DTIM and TIM beacons, the receiving mode is consistently set to S1G_1M preamble format with Long GI, MCS of 0, and a channel bandwidth of 1 MHz, as indicated in the packet. These settings remain unchanged in MM6108, regardless of variations in bandwidth or MCS. However, real-world measurements reveal slight differences in the time and energy consumption required to receive DTIM and TIM beacons within different bandwidths, as summarized in Table 3.

We denote the time required to receive the DTIM beacon and TIM beacon as t_{DTIM} , t_{TIM} , respectively. The total duration of the receiving state, denoted as t_{RX} , is expressed as:

$$t_{RX} = t_{DTIM} + 2t_{TIM} + t_{ACK}. \quad (9)$$

Similarly, the energy required to receive the DTIM beacon is denoted as E_{DTIM} , while the energy required to receive the TIM beacon is denoted as E_{TIM} . The total energy consumption during the receiving state, denoted as E_{RX} , can be expressed as:

$$E_{RX} = E_{DTIM} + 2E_{TIM} + E_{ACK}. \quad (10)$$

3) IDLE STATE

Referring to Figure 3, the IDLE time is equal to the time of waiting for three beacon intervals minus the time spent in transmitting and the time spent in receiving. Denoting the beacon interval as t_{beacon} and the IDLE state duration as t_{IDLE} , t_{IDLE} can be expressed as:

$$t_{IDLE} = 3t_{beacon} - t_{TX} - t_{RX}. \quad (11)$$

The energy consumption during the IDLE state, denoted as E_{IDLE} , can be expressed as:

$$E_{IDLE} = I_{IDLE} \cdot t_{IDLE} \cdot V. \quad (12)$$

where V is the supply voltage, I_{IDLE} is the current during the IDLE state, and t_{IDLE} is the duration of the IDLE state.

4) OVERALL ENERGY AND TIME OF ACTIVE PHASE

After analyzing the energy consumption of the three individual states, the total energy consumption during the Active phase, denoted as E_{Active} , can be calculated as the sum of the energy consumption of the transmitting, receiving, and IDLE states. This can be expressed as:

$$E_{Active} = E_{TX} + E_{RX} + E_{IDLE}. \quad (13)$$

where E_{TX} , E_{RX} , and E_{IDLE} represent the energy consumption during the transmitting, receiving, and IDLE states, respectively.

Similarly, the total time spent during the Active phase, denoted as t_{Active} , is the sum of the durations of the transmitting, receiving, and IDLE states. This can be expressed as:

$$t_{Active} = t_{TX} + t_{RX} + t_{IDLE}. \quad (14)$$

where t_{TX} , t_{RX} , and t_{IDLE} represent the time durations of the transmitting, receiving, and IDLE states, respectively.

C. ENERGY CONSUMPTION OF TO SLEEP PHASE

In toSleep phase, the STA performs several tasks to transition from the Active state to the Sleep state. These tasks include disabling its transceiver, saving necessary state information for the next wake-up cycle, and powering down non-essential components to minimize energy consumption.

The duration and energy consumption of the toSleep phase are influenced not only by the MCS and bandwidth configurations but also by the hardware characteristics of the STA. Similar to the toActive phase, it is challenging to model this phase using a purely mathematical formula. Therefore, we adopt the same measurement-based approach, conducting 50 measurements under different bandwidths and MCS settings and taking the average values. The duration of the toSleep phase, $t_{toSleep}$, was measured to be an average of 1.05 ms. The average energy consumption for this phase, $E_{toSleep}$, is 0.03 mJ. These values are expressed as follows:

$$t_{toSleep} = 1.05 \text{ ms}, \quad (15)$$

$$E_{toSleep} = 0.03 \text{ mJ}. \quad (16)$$

D. ENERGY CONSUMPTION OF SLEEP PHASE

The duration of the Sleep phase, denoted as t_{Sleep} , can be calculated as the duration of wake interval ($t_{interval}$) minus the durations of the Wake-up phases ($t_{toActive}$, t_{Active} , and $t_{toSleep}$). This relationship is expressed as:

$$t_{Sleep} = t_{interval} - t_{toActive} - t_{Active} - t_{toSleep}. \quad (17)$$

During the Sleep phase, the STA operates at a minimal current level, denoted as I_{Sleep} . The energy consumption during the Sleep phase, E_{Sleep} , can be calculated using the formula:

$$E_{Sleep} = I_{Sleep} \cdot t_{Sleep} \cdot V. \quad (18)$$

where I_{Sleep} represents the current during the Sleep phase, V is the supply voltage, and t_{Sleep} is the sleep duration.

E. ENERGY CONSUMPTION OF FEM

The FEM is primarily active during the data transmission period. Let I_{FEM} represent the current consumption of the FEM while transmitting, the energy consumption of the FEM during the wake interval, denoted as E_{FEM} , can be calculated using:

$$E_{\text{FEM}} = I_{\text{FEM}} \cdot t_{\text{TX}} \cdot V. \quad (19)$$

where V is the supply voltage.

F. TOTAL ENERGY CONSUMPTION

To obtain the total energy consumption of the STA during a single wake interval, we sum the energy consumed by the core chip across all four operational phases and the energy consumed by the FEM. The total energy consumption, denoted as E_{Total} , is given by:

$$E_{\text{Total}} = E_{\text{toActive}} + E_{\text{Active}} + E_{\text{toSleep}} + E_{\text{Sleep}} + E_{\text{FEM}}. \quad (20)$$

IV. RESULTS AND ANALYSIS

This section presents the results obtained from experiments to validate the accuracy of our energy consumption modeling when the TWT function is enabled. Throughout all experiments, the wake duration is set to 60 ms, and the TWT wake interval is set to 5,119.98 ms. Setting the TWT interval as a multiple of the beacon interval (102.3996 ms) ensures that the STA wakes up at precise intervals.

A. MODEL VALIDATION

In the previous section, a mathematical model was established to predict the energy consumption of Wi-Fi HaLow devices when the TWT function is enabled. To ensure its accuracy and applicability in real-world scenarios, experimental validation is necessary. Initially, it was assumed that the transmission (I_{TX}), reception (I_{RX}), and IDLE (I_{IDLE}) currents remained constant across different configurations. This assumption was used in the mathematical model to estimate energy consumption. However, discrepancies were observed between the model-predicted energy values and the actual measured consumption. Further investigation revealed that current consumption is not static but varies dynamically with the MCS and bandwidth settings. Both the core module and the front-end module exhibit varying current levels depending on these parameters. Table 4 and Table 5 presents the measured current values under different MCS and bandwidth configurations. Notably, the current in sleep state remains consistently low at approximately 112 μA , regardless of MCS and bandwidth settings.

By recalculating energy consumption using the experimentally obtained current values, a set of model-predicted energy values was obtained. These results were then compared with the actual measured energy consumption under different MCS and bandwidth configurations, which are presented in Tables 6 to 9, detailing the measured energy consumption (E_m) and model-predicted energy consumption

TABLE 4. Measured current values (I_{TX} , I_{RX} , I_{IDLE}) across Different bandwidths and MCS settings of core module.

bandwidth	MCS	I_{TX} (mA)	I_{RX} (mA)	I_{IDLE} (mA)
1MHz	0	61.22	32.52	32.37
	1	61.27	32.47	32.33
	2	61.20	32.56	32.38
	3	56.08	32.59	32.38
	4	56.07	32.59	32.42
	5	55.03	32.58	32.42
	6	52.84	32.61	32.42
	7	51.15	32.60	32.40
2MHz	0	64.53	34.94	33.87
	1	64.84	34.92	33.80
	2	64.85	34.84	33.81
	3	59.75	34.86	33.81
	4	59.77	35.00	33.81
	5	58.91	35.00	33.80
	6	56.55	34.83	33.78
	7	54.77	35.04	33.78
4MHz	0	70.75	40.72	37.57
	1	71.28	40.56	37.56
	2	71.35	40.67	37.60
	3	66.79	40.62	37.62
	4	67.21	40.62	37.61
	5	66.46	40.75	37.62
	6	64.32	40.80	37.62
	7	62.81	40.67	37.71
8MHz	0	85.24	43.84	43.21
	1	86.65	44.12	43.16
	2	86.40	44.06	43.13
	3	81.54	44.16	43.13
	4	81.39	44.05	43.13
	5	80.07	43.74	43.18
	6	77.21	44.18	43.26
	7	77.09	44.13	43.27

TABLE 5. Measured transmission current I_{TX} (mA) across different bandwidths and MCS settings of front-end module when TX power = 24 dBm.

MCS	1MHz	2MHz	4MHz	8MHz
0	365	364	355	353
1	364	362	354	352
2	363	361	352	350
3	311	309	302	300
4	310	308	302	300
5	297	295	288	287
6	277	275	271	270
7	265	265	260	260

(E_p) for various configurations.¹ These include different bandwidths (1 MHz, 2 MHz, 4 MHz, and 8 MHz), data

¹When the bandwidth is set to 1 MHz and MCS is 0, transmitting 800 bytes and 1000 bytes results in fragmentation. Since the TWT mechanism on SX-SDMAH lacks a fixed rule for handling fragmented, meaning that the number and size of fragments cannot be predicted, the energy consumption during fragmentation cannot be accurately estimated. Therefore, energy values in such cases are marked as N/A.

TABLE 6. Energy consumption at 1 MHz bandwidth for different data sizes and MCS.

data size	MCS	E_m (mJ)	E_p (mJ)	AE (mJ)	RE (%)
500 bytes	0	57.61	57.01	0.60	1.05
	1	47.56	47.15	0.41	0.87
	2	44.17	43.87	0.30	0.68
	3	41.43	41.26	0.17	0.41
	4	40.01	39.86	0.15	0.38
	5	39.05	39.00	0.05	0.13
	6	38.58	38.52	0.06	0.16
800 bytes	7	38.27	38.21	0.06	0.16
	0	N/A	N/A	N/A	N/A
	1	52.12	51.81	0.31	0.60
	2	47.39	46.97	0.42	0.89
	3	43.40	43.24	0.16	0.37
	4	41.39	41.20	0.19	0.46
	5	40.03	39.97	0.06	0.15
1000 bytes	6	39.68	39.33	0.35	0.89
	7	39.02	38.88	0.14	0.36
	0	N/A	N/A	N/A	N/A
	1	55.35	54.95	0.40	0.73
	2	49.52	49.07	0.45	0.92
	3	44.83	44.56	0.27	0.61
	4	42.24	42.06	0.18	0.43
1000 bytes	5	40.82	40.56	0.26	0.64
	6	40.10	39.86	0.24	0.60
	7	39.53	39.35	0.18	0.46

sizes (500 bytes, 800 bytes, and 1000 bytes), and MCS (0-7) levels. To evaluate the accuracy of our modeling, both absolute error (AE) and relative error (RE) are included in our computations. This can provide different insights into the accuracy and reliability of numerical results.

From Tables 6 and 7, we can see that the model demonstrates a high level of accuracy at both 1 MHz and 2 MHz bandwidths, where the differences between E_m and E_p are minimal. Across these two bandwidths, AE values are consistently low, typically below 0.3 mJ, and RE rarely exceed 0.7%. This consistent performance indicates that the model effectively captures the energy dynamics for lower (narrower) bandwidths like 1 MHz and 2 MHz, maintaining reliable predictions regardless of data size or MCS. These results validate the robustness of the model for scenarios involving narrower channel widths.

At 4 MHz bandwidth, the model achieves its highest level of accuracy, with AE and RE values being the lowest among all scenarios. The data presented in Table 8 clearly illustrate this superior performance, with AE consistently below 0.14 mJ and RE often under 0.26%. Notably, for data size of 1000 bytes, the relative error is limited to 0.28%. The model also maintains consistency across smaller data sizes, such as 500 bytes, where the RE remaining well below 0.29%. The consistently low AE and RE values indicate that 4 MHz represents an optimal bandwidth for the model's energy prediction capabilities.

The model's performance at 8 MHz bandwidth, as shown in Table 9, demonstrates slightly higher deviations compared

TABLE 7. Energy consumption at 2 MHz bandwidth for different data sizes and MCS.

data size	MCS	E_m (mJ)	E_p (mJ)	AE (mJ)	RE (%)
500 bytes	0	48.92	48.59	0.33	0.68
	1	43.60	43.48	0.12	0.28
	2	41.94	41.75	0.19	0.46
	3	40.47	40.31	0.16	0.40
	4	39.71	39.57	0.14	0.35
	5	39.16	39.08	0.08	0.20
	6	38.86	38.79	0.07	0.18
800 bytes	7	38.71	38.63	0.08	0.21
	0	53.36	52.91	0.45	0.85
	1	45.91	45.63	0.28	0.61
	2	43.40	43.15	0.25	0.58
	3	41.31	41.22	0.09	0.22
	4	40.24	40.17	0.07	0.17
	5	39.60	39.54	0.06	0.15
1000 bytes	6	39.27	39.15	0.12	0.31
	7	39.08	38.91	0.17	0.44
	0	56.23	55.81	0.42	0.75
	1	47.22	47.07	0.15	0.32
	2	44.39	44.12	0.27	0.61
	3	41.95	41.85	0.10	0.24
	4	40.76	40.57	0.19	0.47
1000 bytes	5	40.00	39.84	0.16	0.40
	6	39.55	39.40	0.15	0.38
	7	39.27	39.14	0.13	0.33

to narrower bandwidths. AE values, while higher, remain consistently below 0.37 mJ, and RE are generally under 0.7%. This slight increase in error may be attributed to the complexities of energy dynamics associated with wider bandwidths. Nonetheless, the model still aligns closely with measured values, exhibiting strong predictive accuracy. Such results affirm the model's adaptability and reliability for diverse wireless communication scenarios, including high-bandwidth applications.

B. DISCREPANCIES AND INSIGHTS

The discrepancies between the predicted energy consumption (E_p) and the measured energy consumption (E_m) can be attributed to several factors. These factors include hardware-induced variations, environmental influences, and power transition states.

1) HARDWARE LIMITATIONS

The discrepancy can be partially attributed to inherent instability in hardware behavior. Real devices exhibit power fluctuations due to factors such as circuit inefficiencies, leakage currents, and transient behaviors in voltage regulators and radio frequency (RF) amplifiers. These variations arise from aging effects in circuit components, and temperature-dependent performance shifts. For instance, leakage currents can increase as the device temperature rises, affecting standby power consumption, while voltage regulators and RF amplifiers may exhibit nonlinear efficiency characteristics under varying load conditions.

TABLE 8. Energy consumption at 4 MHz bandwidth for different data sizes and MCS.

data size	MCS	E_m (mJ)	E_p (mJ)	AE (mJ)	RE (%)
500 bytes	0	48.12	47.98	0.14	0.29
	1	45.21	45.11	0.10	0.22
	2	44.20	44.12	0.08	0.18
	3	43.30	43.25	0.05	0.12
	4	42.87	42.81	0.06	0.14
	5	42.55	42.52	0.03	0.07
	6	42.41	42.36	0.05	0.12
	7	42.34	42.32	0.02	0.05
800 bytes	0	50.19	50.06	0.13	0.26
	1	46.20	46.16	0.04	0.09
	2	44.90	44.82	0.08	0.18
	3	43.77	43.73	0.04	0.09
	4	43.24	43.13	0.11	0.26
	5	42.79	42.76	0.03	0.07
	6	42.62	42.54	0.08	0.19
	7	42.47	42.46	0.01	0.02
1000 bytes	0	51.56	51.44	0.12	0.23
	1	46.87	46.84	0.03	0.06
	2	45.39	45.28	0.11	0.24
	3	44.10	43.99	0.11	0.25
	4	43.44	43.32	0.12	0.28
	5	42.89	42.85	0.04	0.09
	6	42.73	42.64	0.09	0.21
	7	42.58	42.55	0.03	0.07

TABLE 9. Energy consumption at 8 MHz bandwidth for different data sizes and MCS.

data size	MCS	E_m (mJ)	E_p (mJ)	AE (mJ)	RE (%)
500 bytes	0	51.91	51.60	0.31	0.60
	1	50.05	49.72	0.33	0.66
	2	49.34	48.97	0.37	0.76
	3	48.68	48.34	0.34	0.70
	4	48.35	48.08	0.27	0.56
	5	48.10	47.85	0.25	0.52
	6	47.87	47.80	0.07	0.15
	7	47.86	47.72	0.14	0.29
800 bytes	0	52.80	52.59	0.21	0.40
	1	50.50	50.18	0.32	0.64
	2	49.67	49.29	0.38	0.77
	3	48.86	48.54	0.32	0.66
	4	48.48	48.19	0.29	0.60
	5	48.23	47.96	0.27	0.56
	6	48.11	47.89	0.22	0.46
	7	48.03	47.79	0.24	0.50
1000 bytes	0	53.38	53.19	0.19	0.36
	1	50.86	50.53	0.33	0.65
	2	49.91	49.54	0.37	0.75
	3	49.01	48.71	0.30	0.62
	4	48.64	48.31	0.33	0.68
	5	48.36	48.04	0.32	0.67
	6	48.26	47.96	0.30	0.63
	7	48.14	47.85	0.29	0.61

2) ENVIRONMENTAL AND CHANNEL CONDITIONS

The established energy model based on ideal transmission, yet real-world deployments are influenced by external conditions such as multipath fading, interference, and signal attenuation, which affect transmission efficiency and power consumption. Although this study's deployment was designed to minimize environmental factors as much as possible, their influence remains unavoidable. Moreover, external RF interference from coexisting wireless systems introduce additional unpredictability, leading to variations in transmission duration and retransmission overheads. These factors, which are difficult to account for in a theoretical model, can result in observable discrepancies between predicted and measured energy consumption.

3) POWER STATE TRANSITIONS

The dynamic nature of power state transitions also plays a critical role in the differences between E_p and E_m . When STA transitions between sleep and active states, the associated energy cost is inherently unpredictable, sometimes exhibiting larger fluctuations despite its relatively small contribution to overall energy consumption. Additionally, during data transmission, the current must switch from IDLE state to TX state and, after completion, transition back to IDLE. These current changes incur additional energy costs, which are difficult to model precisely. Over multiple transmissions, these small discrepancies accumulate, leading to measurable deviations from the predicted values.

C. ANALYSIS OF KEY INFLUENCING FACTORS

To provide a more intuitive visualization of how MCS level, bandwidth, and data size influence energy consumption, the data of predicted and measured energy consumption from Tables 6 to 9 are represented in Figure 5.

From Figure 5, it is evident that MCS level has a significant impact on energy consumption. At lower MCS levels, the transmission rate is relatively low, leading to prolonged transmission durations and, consequently, higher energy consumption. In contrast, higher MCS levels allow for faster data transmission, reducing the active transmission time and minimizing the overall energy cost. This pattern is consistent across all bandwidths, though the rate of decrease varies. However, it is important to note that although higher MCS levels are more energy-efficient, they require better channel conditions to maintain successful transmission.

The impact of bandwidth on energy consumption varies with the MCS level. At lower MCS levels, narrower bandwidths (1 MHz and 2 MHz) exhibit higher energy consumption compared to wider bandwidths (4 MHz and 8 MHz) due to prolonged transmission durations. As the MCS level higher (beyond 3), narrower bandwidths become more energy-efficient than wider bandwidths. This transition occurs because, at high MCS levels, the reduction in circuit power consumption for narrower bandwidths outweighs the advantage of shorter transmission times in wider bandwidths. Moreover, the decline in energy consumption follows distinct patterns, with wider bandwidths experiencing a sharp

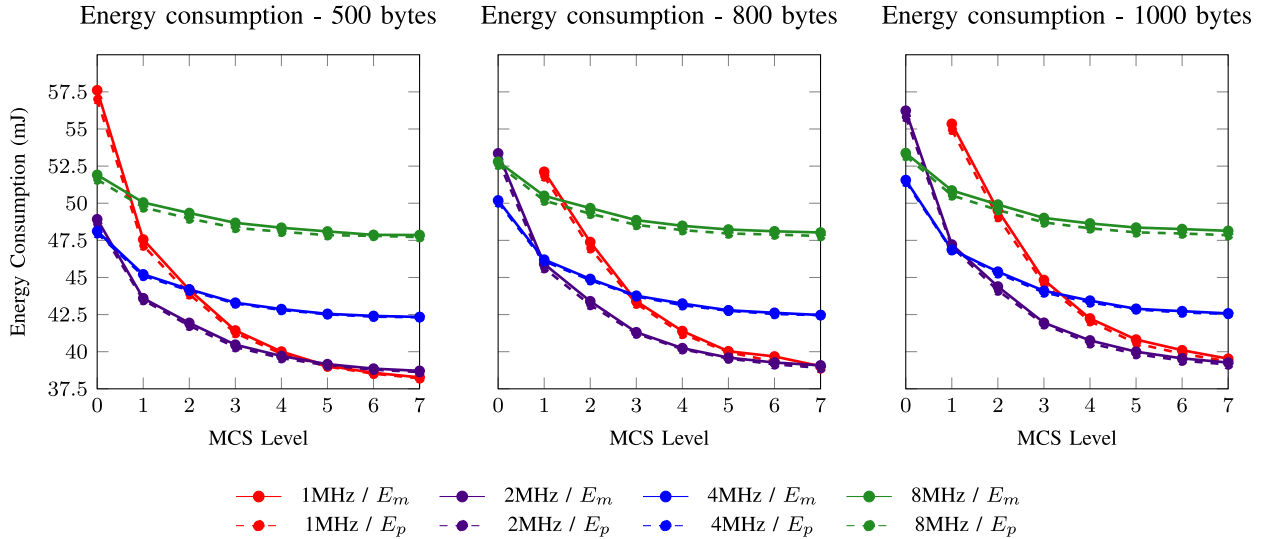


FIGURE 5. Predicted (E_p) and Measured (E_m) energy consumption across MCS Levels, bandwidths, and data sizes. The strong agreement between model predictions and real measurements across all configurations validates the model's ability to accurately capture energy consumption behavior under different transmission conditions.

decrease at lower MCS levels, while narrower bandwidths show a consistent downward trend across the entire MCS range.

Data size also influences energy consumption, though the increase in energy is not proportional to the increase in data size. As the data size grows from 500 bytes to 800 bytes and 1000 bytes, energy consumption increases, but the increments are relatively small. This indicates that a significant portion of the total energy consumption is attributed to non-data transmission activities, such as waiting in IDLE state.

The data presented in Tables 6 to 9 represent the total energy consumption of both the core chip and the FEM. To further investigate the impact of MCS level, bandwidth, and data size on each module separately, we calculated and measured their energy consumption individually, as illustrated in Figures 6 and 7. For a more intuitive comparison, we present the results in line charts, as shown in Figures 8 and 9.

As observed in Figure 8, there is a significant difference in energy consumption across different bandwidths, with higher bandwidths exhibiting greater energy consumption. This is primarily because data transmission occupies only a small portion of the TWT wake interval, while a substantial part of the energy is consumed during the IDLE state. According to Table 4, the current values of both transmission and IDLE state vary considerably across different bandwidths, with higher bandwidths leading to higher current consumption in both states. However, for a given bandwidth, the IDLE state current remains nearly constant, which explains why Figure 8 shows only minor variations in energy consumption as MCS increases within the same bandwidth. Therefore, to reduce the energy consumption of the core module, it is essential to minimize bandwidth usage. Additionally, utilizing higher MCS levels where possible can slightly reduce energy consumption by shortening transmission durations.

The energy consumption of the FEM is entirely determined by the energy used for data transmission, making transmission duration and current value the key influencing factors. As shown in Table 4, for a given bandwidth, higher MCS levels correspond to lower transmission currents, whereas at a fixed MCS level, variations in bandwidth have minimal impact on current. However, transmission duration is significantly affected by both MCS and bandwidth—higher MCS levels and wider bandwidths lead to shorter transmission durations. Consequently, Figure 9 demonstrates that for the same MCS level, wider bandwidths exhibit lower energy consumption, and for the same bandwidth, increasing MCS levels reduces energy consumption. Furthermore, as MCS continues to increase, energy consumption gradually stabilizes. This trend arises because at sufficiently high MCS levels, transmission duration becomes extremely short, making the baseline transmission power the dominant factor rather than further reductions in time. Therefore, to minimize FEM energy consumption, maximizing MCS levels is an effective strategy, as it reduces transmission time while maintaining transmission efficiency. Additionally, using a wider bandwidth is beneficial when conditions allow, as it significantly reduces transmission time, further lowering energy consumption.

D. PRACTICAL RECOMMENDATIONS

The total energy consumption is determined by the combined energy usage of the core chip and the FEM. The core chip primarily consumes energy in the IDLE state, making lower bandwidth and higher MCS configurations preferable for reducing its energy consumption. However, a lower bandwidth increases the data transmission time, leading to a substantial rise in FEM energy consumption, which is undesirable in battery-powered sensor applications.

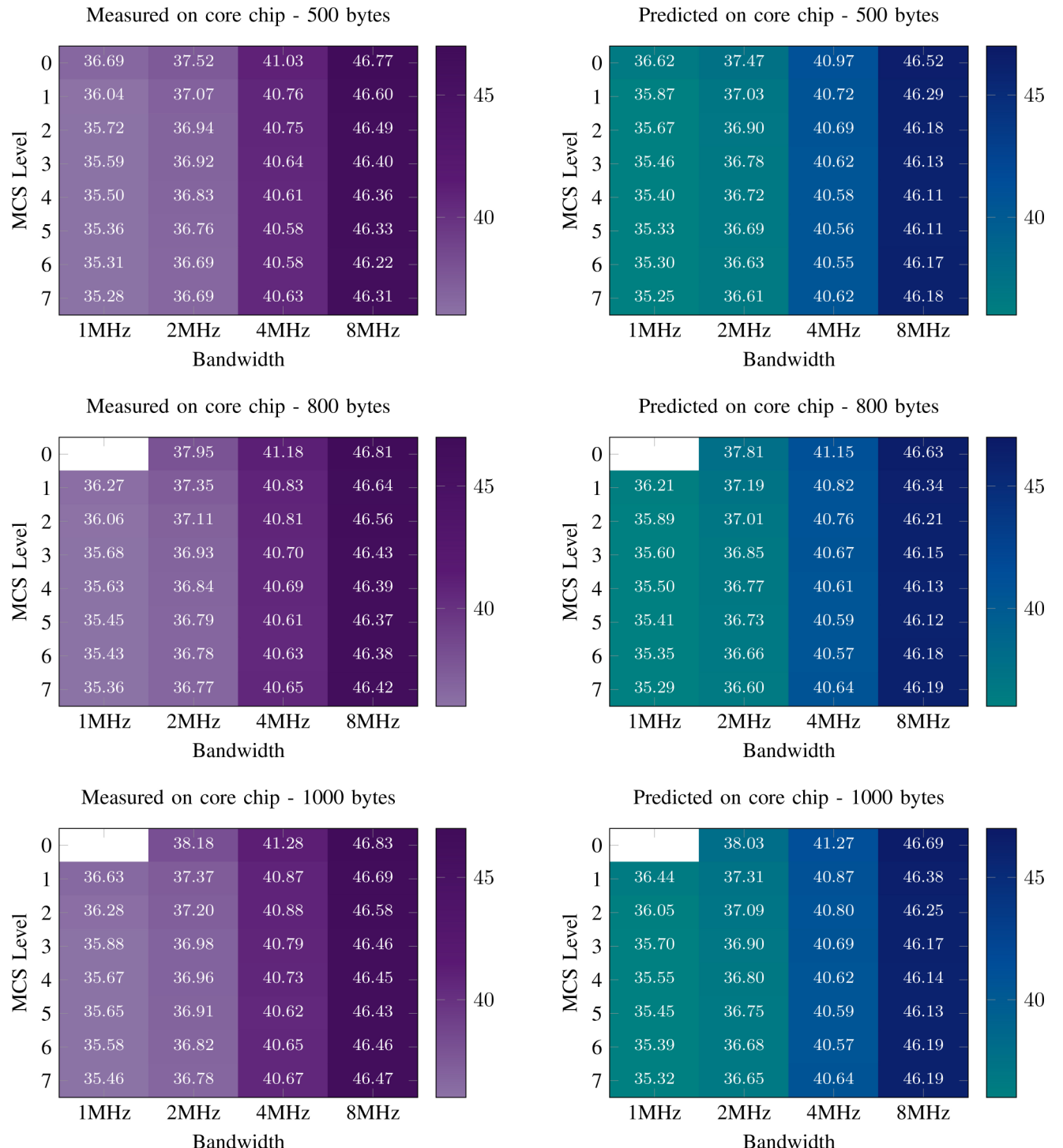


FIGURE 6. Measured and predicted energy consumption (mJ) on the core chip across MCS levels, bandwidths, and data sizes. The predicted values closely align with the measured results across different configurations, validating the model's accuracy. Blank cells indicate N/A values where experimental data were unavailable.

To minimize FEM energy consumption, lowering transmission power and reducing transmission time are two viable strategies. As demonstrated by Maudet et al., reducing transmission power leads to lower transmission current [22], thereby decreasing FEM energy consumption. Nevertheless, this must be balanced against the risk of transmission

failures. Under poor channel conditions, reducing transmission power will increase the packet error rate [30], leading to retransmissions and ultimately higher energy consumption. As for transmission time, it can be reduced by increasing bandwidth, selecting a higher MCS, or a combination of both. However, wide bandwidth and high MCS settings

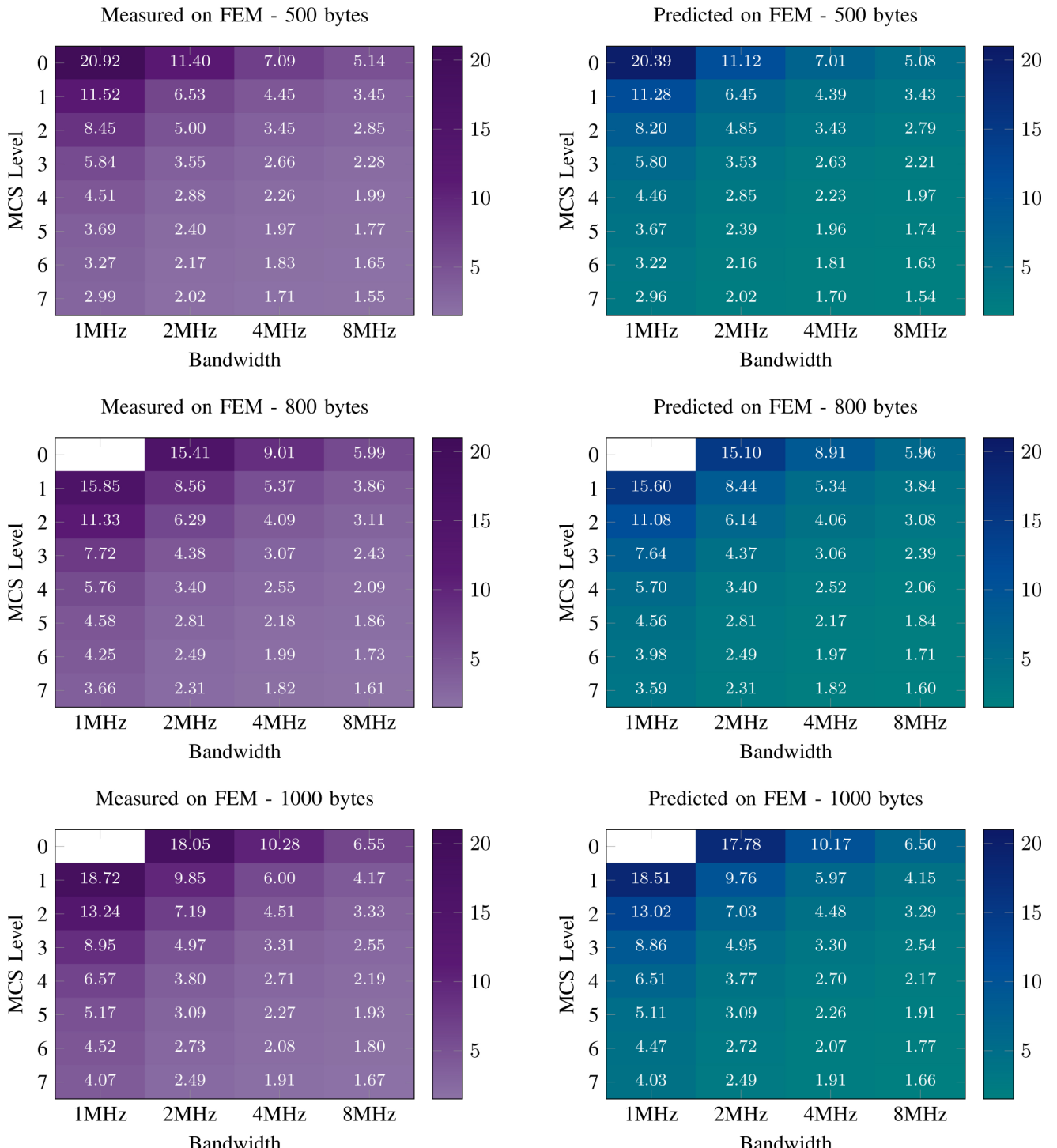


FIGURE 7. Measured and predicted energy consumption (mJ) of FEM across MCS levels, bandwidths, and data sizes. The results show strong alignment between model predictions and actual measurements across all configurations. Blank cells indicate N/A values where experimental data were unavailable.

can degrade transmission reliability in long-range deployments [10], making them unsuitable for communication over extended distances.

Given the distinct energy characteristics of core chip and FEM modules, manufacturers should impose firmware restrictions on the maximum allowable transmission duration under the TWT mechanism. Meanwhile, network operators

should aim to enhance energy efficiency by choosing low bandwidth, high MCS, and low transmission power whenever possible, provided that packet delivery rate remain adequately maintained.

Another recommendation in energy efficiency is the scheduling of data transmission within TWT wake interval. When a STA needs to transmit a certain amount of data, it

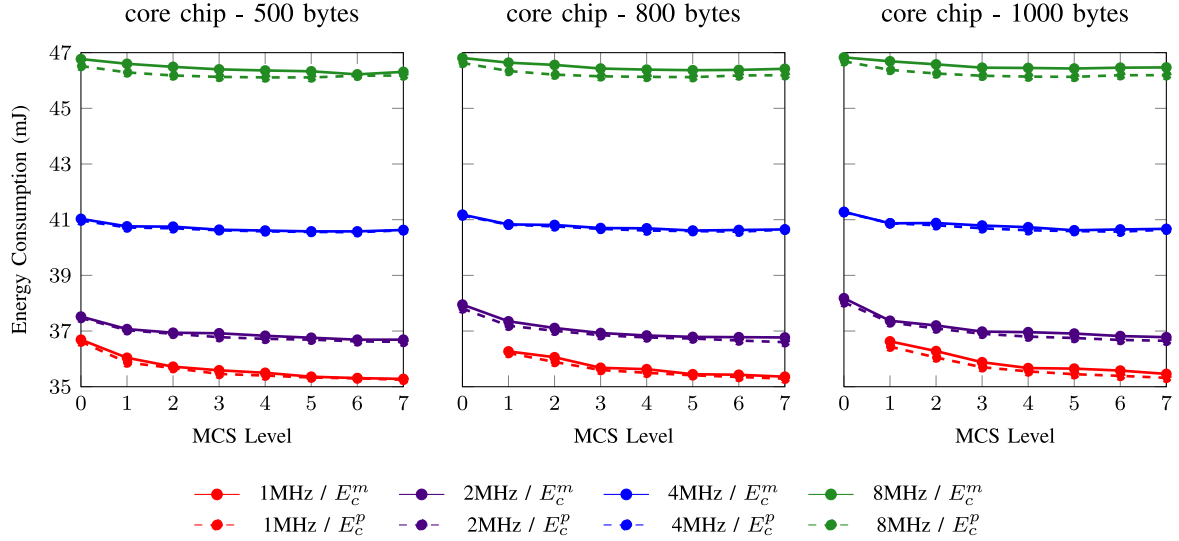
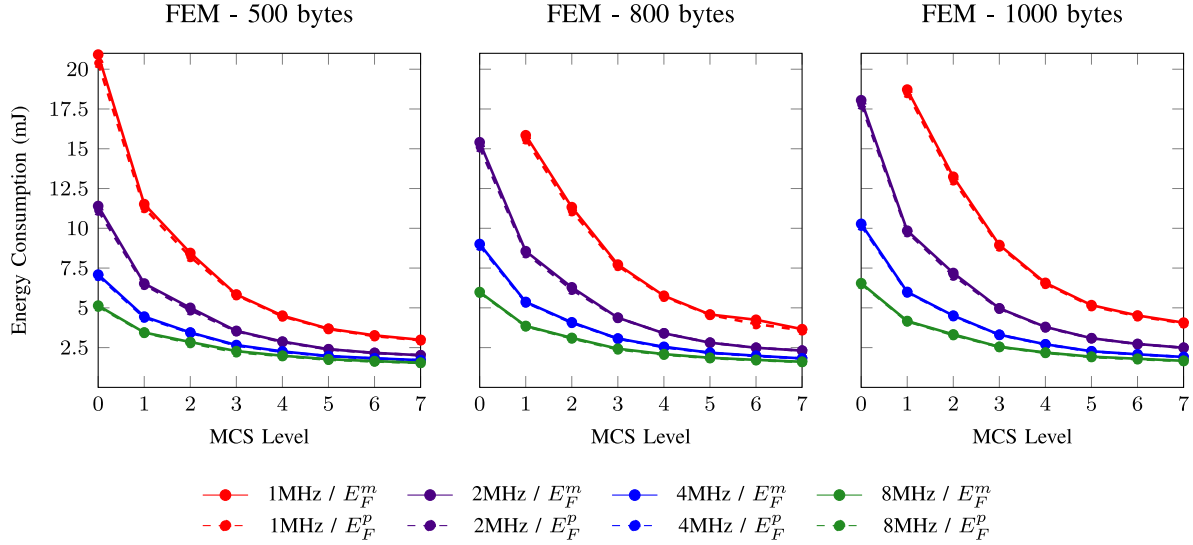


FIGURE 8. Predicted (E_c^p) and Measured (E_c^m) energy consumption of core chip across MCS Levels, bandwidths, and data sizes. Energy consumption decreases significantly with increasing MCS levels up to MCS 3, beyond which the reduction becomes marginal. Larger bandwidths result in higher energy usage.



is advantageous to ensure that the transmission is completed within a single wake interval rather than being distributed across multiple cycles. Splitting transmissions over multiple cycles incurs additional energy consumption of staying in the IDLE state, which significantly impacts overall efficiency.

While the recommendations proposed in this paper are derived from controlled experiments, we acknowledge that real-world deployments often involve additional factors such as channel interference, mobility-induced variations, and reliability concerns like retransmissions or packet loss. These factors were intentionally excluded to eliminate the influence of non-TWT-related variables, allowing us to focus on analyzing the intrinsic energy behavior of the TWT mechanism itself. Nevertheless, our findings serve as a foundational reference,

and future work will incorporate these trade-offs to improve the robustness and applicability of the recommendations under dynamic and realistic deployment scenarios.

E. LESSONS LEARNED

1) CURRENT CONSUMPTION VARIES WITH DEVICE STATE AND NETWORK CONFIGURATION

One of the key findings in this study is that current consumption is not constant but varies dynamically depending on device state and network configuration. The transmission, reception, and IDLE states exhibit distinct current levels, and these values further change related to different MCS levels and bandwidth options. Given these variations, energy consumption calculations must incorporate state-specific current

measurements for each configuration rather than assuming fixed current values. Moreover, since transmission power directly impacts transmission current, energy evaluations under different power settings must use corresponding transmission current values to ensure accuracy. These findings emphasize the need for precise current profiling when modeling energy consumption of Wi-Fi HaLow networks.

2) SCENARIOS WHERE TWT IS EFFECTIVE

The TWT mechanism is designed to maximize energy efficiency by allowing devices to remain in sleep mode for extended periods and wake up only when necessary for scheduled data transmissions. This makes TWT highly effective in scenarios where traffic is predictable and consists of small amounts of data transmitted at regular intervals, such as IoT sensor networks, industrial monitoring, and smart agriculture.

If traffic is unpredictable or frequent, such as in real-time communication, video streaming, or applications with bursty traffic, TWT scheduling may lead to inefficiencies, as devices might miss unscheduled transmissions or wake up too frequently. If the data payload is big, multiple TWT wake intervals may be required to complete the transmission. This leads to additional and unnecessary energy consumption. In such cases, alternative energy-saving strategies may be more effective. Therefore, a clear understanding of traffic characteristics is essential before deciding whether TWT should be implemented.

In addition to requiring an accurate prediction of traffic, configuring the system with low bandwidth, high MCS, and low transmission power can further enhance the energy-saving potential of the TWT mechanism. However, high MCS and low transmission power can reduce transmission reliability, making TWT less suitable for long-range communication. This limitation contradicts one of Wi-Fi HaLow's inherent advantages—its capability for long-distance transmission. As a result, when TWT is applied in long-distance scenarios, the efficiency of energy savings is inevitably compromised. Therefore, in cases where devices are highly energy-constrained and battery replacement is impractical, it is advisable to minimize communication distances whenever possible to ensure optimal energy efficiency.

V. DISCUSSION AND FUTURE WORKS

A. MODEL IMPROVEMENTS OVER EXISTING APPROACHES

Prior simulation-based energy models typically assume constant current draw and lack the resolution to distinguish energy use across different hardware components and protocol phases. Our proposed model improves upon these limitations by using empirical current measurements from actual Wi-Fi HaLow hardware. It accounts for variable power consumption based on bandwidth, MCS, and device state, and separates energy contributions of the core chip and FEM. This enables more precise, phase-specific modeling that better supports optimization and deployment in real-world low-power wireless systems.

B. HARDWARE DEPENDENCE AND MODEL GENERALIZABILITY

This study employs the Morse Micro MM6108 chipset as the experimental platform. At the time of conducting this research, MM6108 was the only commercially available Wi-Fi HaLow chipset that supported the TWT mechanism. Although the empirical values in our model are chipset-specific, the modeling framework itself is designed to capture the behavioral structure of TWT operation, such as wake-up, synchronization, data transmission, and return to sleep. These transitions are determined by the TWT protocol itself rather than the specific hardware. As a result, the phase-based modeling methodology proposed in this work provides a transferable framework that can serve as a reference for other TWT-capable chipsets once they become available, such as those from Newracom.

C. ADAPTABILITY TO VARIABLE TWT INTERVALS

Although the MM6108 chipset used in our experiments only supports implicit TWT scheduling with a fixed interval, our proposed model is inherently designed to accommodate variable TWT intervals. Specifically, the model is modular and phase-based, with the TWT interval treated as a configurable variable rather than a fixed constant. This design enables energy prediction under both static and adaptive TWT schedules. For applications requiring dynamic wake-up intervals, such as emergency alerts, the model can compute the total energy consumption by directly updating the interval input, without the need to reconstruct or redesign the model structure. This flexibility extends the applicability of our model to a broader range of real-world deployment scenarios, beyond what is directly supported by the current hardware.

D. IDEALIZED ASSUMPTION AND REALISTIC CONDITIONS

The current model assumes ideal channel conditions with no packet loss or retransmission. While this assumption allows for clearer interpretation of TWT phase-level energy behavior, it may not hold in real-world environments where channel congestion, interference, or fading occurs. In such cases, retransmissions due to failed ACKs or collisions may increase energy usage. Although such dynamics are beyond the scope of this initial modeling effort, future extensions could incorporate stochastic models of packet error rate or real world trace-based validation to improve realism.

E. ENERGY PROFILE DRIFT OVER DEVICE LIFETIME

Although our energy model was developed and validated under short-term, stable conditions, we acknowledge that long-term hardware aging may impact power consumption characteristics over time. Factors such as battery degradation [31] and temperature-induced stress [32] can lead to gradual shifts in baseline current levels. These effects are not captured in the current model, which focuses on isolating the protocol-induced energy behavior of TWT. However, in long-term deployments, such drift may affect energy

estimation accuracy. Future work could extend the model by incorporating empirical correction factors or periodic calibration mechanisms to account for these lifetime effects. Such enhancements would improve the robustness of the model in real-world, long-term IoT applications.

VI. CONCLUSION

This study presented an empirically validated energy consumption model for Wi-Fi HaLow stations operating under the TWT mechanism. The model was developed based on fine-grained power measurements collected from real Wi-Fi HaLow hardware. By capturing hardware-specific behaviors that are often overlooked in simulation-based research, the model provides a more realistic understanding of energy performance in practical deployment.

The proposed model serves as a valuable tool for both researchers and practitioners. It supports energy-aware protocol design, system-level power optimization, and business-oriented planning, such as forecasting energy requirements and improving cost-efficiency in large-scale IoT networks.

Future work will extend the current model by incorporating factors such as retransmissions and packet loss, which are commonly encountered in real-world deployments and can significantly affect overall energy consumption. The occurrence of such events depends on various environmental and network parameters, and modeling their impact will enable more accurate and application-relevant energy estimation. By considering these dynamic factors, future models will further bridge the gap between theoretical analysis and real deployment scenarios.

REFERENCES

- [1] T. Adame, A. Bel, B. Bellalta, J. Barcelo, and M. Oliver, “IEEE 802.11 AH: the WiFi approach for M2M communications,” *IEEE Wireless Commun.*, vol. 21, no. 6, pp. 144–152, Dec. 2014.
- [2] M. S. Mahmoud and A. A. Mohamad, “A study of efficient power consumption wireless communication techniques/modules for Internet of Things (IoT) applications,” *Adv. Internet Things*, vol. 6, pp. 19–29, Apr. 2016.
- [3] M. Ghamari, H. Arora, R. S. Sherratt, and W. Harwin, “Comparison of low-power wireless communication technologies for wearable health-monitoring applications,” in *Proc. Int. Conf. Comput., Commun., Control Technol. (I4CT)*, 2015, pp. 1–6.
- [4] D. Feng, C. Jiang, G. Lim, L. J. Cimini, G. Feng, and G. Y. Li, “A survey of energy-efficient wireless communications,” *IEEE Commun. Surveys Tuts.*, vol. 15, no. 1, pp. 167–178, 1st Quart., 2012.
- [5] O. Alamu, A. Gbenga-Ilori, M. Adelabu, A. Imoize, and O. Ladipo, “Energy efficiency techniques in ultra-dense wireless heterogeneous networks: An overview and outlook,” *Eng. Sci. Technol., Int. J.*, vol. 23, no. 6, pp. 1308–1326, 2020.
- [6] *IEEE Standard for Information Technology—Telecommunications and Information Exchange Between Systems—Local and Metropolitan Area Networks—Specific Requirements—Part 11: Wireless LAN Medium Access Control (MAC) and Physical Layer (PHY) Specifications*, IEEE Standard 802.11-2020 (Revision of IEEE Std 802.11-2016), 2021.
- [7] L. Kane, V. Liu, M. McKague, and G. Walker, “An experimental field comparison of Wi-Fi HaLow and LoRa for the smart grid,” *Sensors*, vol. 23, no. 17, p. 7409, 2023.
- [8] J. Tosi, F. Taffoni, M. Santacatterina, R. Sannino, and D. Formica, “Performance evaluation of Bluetooth low energy: A systematic review,” *Sensors*, vol. 17, no. 12, p. 2898, 2017.
- [9] M. Park, “IEEE 802.11 ah: sub-1-GHz license-exempt operation for the Internet of Things,” *IEEE Commun. Mag.*, vol. 53, no. 9, pp. 145–151, Sep. 2015.
- [10] B. Domazetović, E. Kočan, and A. Mihovska, “Performance evaluation of IEEE 802.11 ah systems,” in *Proc. 24th Telecommun. Forum (TELFOR)*, 2016, pp. 1–4.
- [11] V. Baños-Gonzalez, M. S. Afraqui, E. Lopez-Aguilera, and E. García-Villegas, “IEEE 802.11 ah: A technology to face the IoT challenge,” *Sensors*, vol. 16, no. 11, p. 1960, 2016.
- [12] A. Šljivo et al., “Performance evaluation of IEEE 802.11 ah networks with high-throughput bidirectional traffic,” *Sensors*, vol. 18, no. 2, p. 325, 2018.
- [13] E. Khorov, A. Lyakhov, A. Krotov, and A. Guschin, “A survey on IEEE 802.11 ah: An enabling networking technology for smart cities,” *Comput. Commun.*, vol. 58, pp. 53–69, Mar. 2015.
- [14] L. Tian, S. Santi, A. Seferagić, J. Lan, and J. Famaey, “Wi-Fi HaLow for the Internet of Things: An up-to-date survey on IEEE 802.11 ah research,” *J. Netw. Comput. Appl.*, vol. 182, May 2021, Art. no. 103036.
- [15] N. Ahmed, D. De, F. A. Barbhuiya, and M. I. Hussain, “MAC protocols for IEEE 802.11 ah-based Internet of Things: A survey,” *IEEE Internet Things J.*, vol. 9, no. 2, pp. 916–938, Jan. 2022.
- [16] E. Guérin, T. Begin, and I. G. Lassous, “An overview of MAC energy-saving mechanisms in WiFi,” *Comput. Commun.*, vol. 203, pp. 129–145, Apr. 2023.
- [17] M. Alam, N. Ahmed, R. Matam, and F. A. Barbhuiya, “Analyzing the suitability of IEEE 802.11 ah for next generation Internet of Things: A comparative study,” *Ad Hoc Netw.*, vol. 156, Apr. 2024, Art. no. 103437.
- [18] T.-L. Kao, H.-C. Wang, C.-H. Lu, and T.-H. Cheng, “An energy consumption evaluation of non-TIM strategy in IEEE 802.11 ah,” *IOP Conf. Ser., Mater. Sci. Eng.*, vol. 644, no. 1, 2019, Art. no. 12008.
- [19] S. Santi, L. Tian, E. Khorov, and J. Famaey, “Accurate energy modeling and characterization of IEEE 802.11 ah RAW and TWT,” *Sensors*, vol. 19, no. 11, p. 2614, 2019.
- [20] S. Santi, L. Tian, and J. Famaey, “Evaluation of the co-existence of RAW and TWT Stations in IEEE 802.11 ah using ns-3,” in *Proc. Workshop Next-Gener. Wireless ns-3*, 2019, pp. 9–12.
- [21] S. Maudet, G. Andrieux, R. Chevillon, and J.-F. Diouris, “Practical evaluation of Wi-Fi HaLow performance,” *Internet Things*, vol. 24, Dec. 2023, Art. no. 100957.
- [22] S. Maudet, G. Andrieux, R. Chevillon, and J.-F. Diouris, “Evaluation and analysis of the Wi-Fi HaLow energy consumption,” *IEEE Internet Things J.*, vol. 11, no. 17, pp. 28244–28252, Sep. 2024.
- [23] S. Aust, “Measurement study of IEEE 802.11 ah sub-1 GHz wireless channel performance,” in *Proc. IEEE 21st Consum. Commun. Netw. Conf. (CCNC)*, 2024, pp. 847–850.
- [24] I.-G. Lee et al., “WiFi HaLow for long-range and low-power Internet of Things: System on chip development and performance evaluation,” *IEEE Commun. Mag.*, vol. 59, no. 7, pp. 101–107, Jul. 2021.
- [25] L. Tian, S. Deronne, S. Latré, and J. Famaey, “Implementation and validation of an IEEE 802.11 ah module for ns-3,” in *Proc. Workshop Ns-3*, 2016, pp. 49–56.
- [26] T. Zhu, Z. Zhong, Y. Gu, T. He, and Z.-L. Zhang, “Leakage-aware energy synchronization for wireless sensor networks,” in *Proc. 7th Int. Conf. Mobile Syst., Appl., Services*, 2009, pp. 319–332.
- [27] L. Gu, J. A. Stankovic et al., “Radio-triggered wake-up capability for sensor networks” in *Proc. IEEE Real-Time Embed. Technol. Appl. Symp.*, 2004, pp. 27–37.
- [28] L. Gu and J. A. Stankovic, “Radio-triggered wake-up for wireless sensor networks,” *Real-Time Syst.*, vol. 29, pp. 157–182, Mar. 2005.
- [29] *IEEE Standard for Information Technology—Telecommunications and Information Exchange between Systems—Local and Metropolitan Area Networks—Specific Requirements—Part 11: Wireless LAN Medium Access Control (MAC) and Physical Layer (PHY) Specifications—Redline*, IEEE Standard 802.11-2020 (Revision of IEEE Std 802.11-2016)—Redline, 2021.
- [30] B. Domazetović and E. Kočan, “Packet error rate in IEEE 802.11 ah use case scenarios,” in *Proc. 25th Telecommun. Forum (TELFOR)*, 2017, pp. 1–4.
- [31] S. Wang et al., “Impact of battery degradation models on energy management of a grid-connected DC microgrid,” *Energy*, vol. 207, Sep. 2020, Art. no. 118228.
- [32] L. M. Rodrigues, C. Montez, G. Budke, F. Vasques, and P. Portugal, “Estimating the lifetime of wireless sensor network nodes through the use of embedded analytical battery models,” *J. Sens. Actuat. Netw.*, vol. 6, no. 2, p. 8, 2017.